Asia-Pacific Journal of Atmospheric Sciences (2024) 60:541–553
https://doi.org/10.1007/s13143-024-00369-1

Online ISSN 1976-7951
Print ISSN 1976-7633

ORIGINAL ARTICLE

# Impacts of Changes in Soil Moisture on Urban Heat Islands and Urban Breeze Circulations: Idealized Ensemble Simulations

**Abeda Tabassum[1] · Seong-Ho Hong[1] · Kyeongjoo Park[1] · Jong-Jin Baik[1]**

Received: 24 December 2023 / Revised: 11 April 2024 / Accepted: 18 May 2024 / Published online: 29 May 2024


## Abstract

Soil moisture plays important roles in land surface and hydrological processes, and its changes can greatly affect weather and climate. In this study, we examine how changes in soil moisture impact the urban heat island (UHI) and urban breeze circulation (UBC) through idealized ensemble simulations. As soil moisture increases, the latent heat flux increases considerably in the rural area. Hence, in the rural area, the sensible heat flux and surface temperature decrease, which decreases the rural air temperature. The decrease in rural air temperature leads to increases in UHI intensity and thus UBC intensity. The urban air temperature also decreases with increasing soil moisture since the cooler rural air is advected to the urban area by the enhanced low-level convergent flow of the UBC. However, the decrease in air temperature is smaller in the urban area than in the rural area. As the UBC intensity increases, the sensible heat flux in the urban area increases. The increase in sensible heat flux in the urban area further increases the UHI intensity. The positive feedback between the UHI intensity and the UBC intensity is revealed when soil moisture increases. The decrease in air temperature in both the urban and rural areas leads to the decrease in planetary boundary layer (PBL) height. As a result, the vertical size of the UBC decreases with increasing soil moisture. As the UBC intensity increases with increasing soil moisture, the advection of water vapor from the rural area to the urban area increases. Combined with the decrease in PBL height, this reduces the water vapor deficit or even leads to the water vapor excess in the urban area depending on soil moisture content.

**Keywords** Soil moisture · Urban heat island · Urban breeze circulation · Ensemble simulations

## 1 Introduction

The urban heat island (UHI) is a phenomenon that the near-surface air temperature is higher in urban areas than in their surrounding rural areas, and it has been extensively studied in cities across the world (Arnfield 2003; Santamouris 2015). The UHI results from the differences in surface energy fluxes between urban and rural areas, that is, larger sensible heat flux, smaller latent heat flux, and larger heat storage in urban areas than in rural areas (Oke 1988; Grimmond and Oke 1999; Piringer et al. 2007; Wang et al. 2015). The urban–rural temperature difference associated with the UHI generates the urban–rural pressure difference which can induce a mesoscale circulation known as the urban breeze circulation (UBC) or UHI-induced circulation (Lemonsu and Masson 2002; Hong et al. 2024). Under calm and clear conditions, the UBC is characterized by the low-level convergent flow toward the urban center and the divergent flow aloft. The convergent flow brings relatively cool and moist rural air to the urban area, and the divergent flow brings relatively warm and dry urban air to the rural area. These convergent and divergent flows modify the spatial distributions of temperature and moisture in the urban area and its surrounding rural area. The horizontal velocity of the UBC can be as strong as 5–7 m $s^{-1}$ in the afternoon and the horizontal size is two to three times larger than the city size (Lemonsu and Masson 2002; Hidalgo et al. 2008b; Ryu et al. 2013a).

Soil moisture is a key factor affecting surface energy fluxes and the characteristics of the planetary boundary layer (PBL) (Pan and Mahrt 1987). The increase in soil moisture enhances the surface evapotranspiration and decreases the surface sensible heat flux (Seneviratne et al. 2010). This decreases the near-surface air temperature (Liu and Pu 2019) and lowers the height of PBL (Findell and Eltahir 2003; Ek and Holtslag 2004). Furthermore, changes in soil moisture can even

✉ Jong-Jin Baik
jjbaik@snu.ac.kr

[1] School of Earth and Environmental Sciences, Seoul National University, Seoul 08826, South Korea

influence heat wave occurrences (Fischer et al. 2007; Hirschi et al. 2011) and precipitation (Hohenegger et al. 2009; Guillod et al. 2015). Given that soil moisture in many regions across the world significantly varies due to climate change, it is necessary to understand how changes in soil moisture affect weather and climate (Xu et al. 2013; Cook et al. 2018).

Changes in soil moisture can significantly affect the UHI (Runnalls and Oke 2000; Martilli 2002; Husain et al. 2014; Schatz and Kucharik 2014). Martilli (2002) reported that the decrease in soil moisture results in faster nighttime cooling in the rural area by reducing the heat capacity of soil and thus increases the nighttime UHI intensity. Husain et al. (2014) examined the diurnal variation of UHI intensity in Oklahoma City under different soil moisture conditions and showed that the increase in rural soil moisture increases the daytime UHI intensity. Several studies investigated the impacts of changes in soil moisture on the interactions between the UHI and heat wave (Ramamurthy and Bou-Zeid 2017; Ramamurthy et al. 2017; Richard et al. 2021). Ramamurthy et al. (2017) analyzed the UHI intensity in New York City during heat waves and showed that the decrease in soil moisture during heat waves is a crucial contributing factor to the synergistic interactions between the UHI and heat waves.

While previous studies have examined the impacts of changes in soil moisture on the UHI, the impacts of changes in soil moisture on the UBC have received little attention despite their importance in urban meteorology and climate. Although it was shown that changes in soil moisture can affect the UBC (Husain et al. 2014), how the size, intensity, and structure of the UBC change with soil moisture is yet to be examined in detail. In addition, the UBC, which is induced by the UHI, can influence the UHI by affecting temperature distributions in and around urban areas. In this regard, the UBC and UHI are interrelated to each other. Hence, it would be interesting to examine feedback between the UBC and UHI when soil moisture changes. This study aims to investigate how changes in soil moisture impact the UHI and UBC through idealized ensemble simulations. Idealized simulations enable us to look into the impacts of changes in soil moisture without the interferences of other influences such as synoptic conditions and geographical features. This helps to understand the essential physical processes associated with the impacts of soil moisture changes on the UHI and UBC. Section 2 describes the numerical model and simulation setup. In Section 3, the results and discussion are presented. Summary and conclusions are given in Section 4.

## 2 Numerical Model and Simulation Setup

Idealized simulations in two dimensions ($x$, $z$) are conducted using the Weather Research and Forecasting (WRF) model version 4.1.3 (Skamarock et al. 2019). The physical parameterization schemes selected for this study are the Dudhia shortwave radiation scheme (Dudhia 1989), the Rapid Radiative Transfer Model (RRTM) longwave radiation scheme (Mlawer et al. 1997), the Yonsei University (YSU) PBL scheme (Hong et al. 2006), the revised MM5 surface layer scheme (Jiménez et al. 2012), the unified Noah land surface model (Tewari et al. 2004), and the WRF single-moment 6-class microphysics scheme (Hong and Lim 2006). To represent physical processes that occur in an urban canopy, a single-layer urban canopy model developed by Ryu et al. (2011) (SNUUCM: Seoul National University Urban Canopy Model) is employed. The SNUUCM adopts a tile approach in calculating urban surface energy fluxes. In this approach, an urban area is subdivided into built-up and natural area fractions. Then, each energy flux for the built-up area fraction is calculated by the SNUUCM and that for the natural area fraction is calculated by the unified Noah land surface model. Finally, the area-weighted averaged energy flux is calculated to obtain the urban surface energy flux.

The computational domain size is 500 km in the horizontal direction and 6 km in the vertical direction. The horizontal grid spacing is 250 m, and the vertical grid spacing increases with height. There are 65 vertical layers, and the height of the lowest model level is 44 m. The uppermost 2 km of the domain is set as the Rayleigh damping layer (Klemp et al. 2008) which acts to absorb gravity waves. Periodic boundary conditions are employed at the lateral boundaries for prognostic variables such as three velocity components, potential temperature, and water vapor mixing ratio. The rotational effect of the earth is neglected. The urban area occupies the central 20 km area of the domain, and the rural area occupies the rest of the domain. The built-up and natural area fractions of the urban area are 0.9 and 0.1, respectively. The values of other urban parameters used in the simulations are the same as those in Ryu et al. (2013a). For instance, the roof width, road width, and mean building height are 15 m. The albedo (emissivity) for roof, road, and wall is 0.2 (0.95). The land use type of the rural area is cropland/woodland mosaic, and that of the urban natural area is cropland/grassland mosaic. The soil type of both rural area and urban natural area is silt loam. Note that the surface properties are identical within the urban area and within the rural area.

To systematically examine the impacts of changes in soil moisture on the UHI and UBC, total 11 experiments with different initial soil moisture contents ranging from 0.15 to 0.40 $m^3\ m^{-3}$ with an equal interval of 0.025 $m^3\ m^{-3}$ are conducted. For each experiment, the same initial soil moisture content is used for both the urban and rural areas. The initial water vapor mixing ratio is 1.5 g $kg^{-1}$ at the surface and decreases linearly with height (0.25 g $kg^{-1}$ at the top of the domain). The initial potential temperature increases with height at a rate of 5 K $km^{-1}$ (298.15 K at the surface).

The initial background wind speed is zero, that is, a resting background state is considered. For each experiment, 10 ensemble simulations are performed (total 110 simulations). Each ensemble member is generated by perturbing initial potential temperature at the three lowest model levels, with random perturbations being between −0.1 and 0.1 K. It is expected to enhance the robustness of our main findings by employing the ensemble method. The latitude is set to be 30°N. The model integration is conducted for 48 h starting from 0000 LST 21 June, with a time step of 1 s. The last 24 h is used for analysis.

The UHI intensity is defined as the difference between the 2-m temperature averaged over the urban area and the 2-m temperature averaged over the rural area. The UBC intensity is defined as the maximum horizontal wind speed in the convergent flow region of the UBC.

## 3 Results and Discussion

### 3.1 Characteristics of the UHI and UBC

Figure 1 shows the ensemble-mean fields of potential temperature anomaly, pressure anomaly, horizontal velocity, and water vapor mixing ratio together with wind vector and vertical velocity at 1300, 1600, and 1900 LST. The initial soil moisture content, denoted by SM hereafter, is 0.25 $m^3$ $m^{-3}$. Here, the potential temperature (pressure) anomaly at each height is the deviation of the potential temperature (pressure) from its horizontal average. At 1300 LST, there are warm anomalies throughout the urban PBL and at upper levels of the rural area (Fig. 1a). The magnitude of the warm anomaly is largest at the urban center. A region of pronounced cold anomaly appears at upper levels of the urban area, which is associated with strong updrafts at the urban center. Below $z \sim 1.5$ km, the pressure anomaly is negative in the urban area and its nearby rural area (Fig. 1d). The magnitude of the negative pressure anomaly is largest near the urban center at $z \sim 0$ km. The horizontal pressure gradient associated with the negative pressure anomaly produces the low-level convergent flow toward the urban center. The urban breeze is well featured by the low-level convergent flow and the upper-level divergent flow (Fig. 1g). At 1300 LST, two urban breeze fronts are located at $x = -1.25$ and 1.50 km and they move toward the urban center. The two urban breeze fronts are eventually merged at 1350 LST, resulting in strong updrafts at the urban center. The horizontal size of the UBC at 1300 LST is 53 km, 2.7 times the urban size, which is similar to the results of previous studies (Hidalgo et al. 2008a; Ganbat et al. 2015). At 1300 LST, the water vapor mixing ratio is generally small in the urban area than in the rural area (Fig. 1j).

At 1600 LST, the urban breeze further intensifies and expands in size horizontally. The warm anomaly at upper levels of the rural area is larger at 1600 LST than at 1300 LST (Fig. 1a and b). The maximum magnitude and horizontal extent of negative pressure anomaly are also larger at 1600 LST (Fig. 1d and e). The UBC is well developed, exhibiting stronger low-level convergent flow, upper-level divergent flow, and updrafts at the urban center (Fig. 1h). The horizontal size of the UBC is much larger (100 km) than that at 1300 LST, and its vertical size is 3.3 km. Due to the enhanced UBC, the water vapor is actively transported toward the urban area from the rural area, upward, and then toward the rural area. At 1600 LST, the water vapor mixing ratio below $z \sim 1.5$ km in the urban area is similar to that in the rural area (Fig. 1k). At 1900 LST, shortly before sunset, the magnitudes of warm anomaly and pressure anomaly are reduced (Fig. 1c and f). The low-level convergent flow in the urban area weakens, while the upper-level divergent flow is still strong (Fig. 1i). Since the transported water vapor is accumulated in the urban area with time, the water vapor mixing ratio throughout the PBL is generally larger in the urban area than in the rural area at 1900 LST (Fig. 1l). The structure and evolution of the UBC described above are qualitatively similar to the results of previous studies (Ryu et al. 2013a; Ganbat et al. 2015; Hong et al. 2024).

The ensemble-mean diurnal variations of net radiation, sensible heat flux, latent heat flux, PBL height, 2-m temperature, and 2-m water vapor mixing ratio averaged over the urban and rural areas are presented in Fig. 2. The sunrise time is 0500 LST and the sunset time is 1904 LST at 30°N on 22 June. In the daytime, the net radiation is similar between the urban and rural areas (Fig. 2a). As discussed in Ryu et al. (2013a), the absorbed shortwave radiation flux is larger in the urban area than in the rural area due to the multiple reflections of shortwave radiation within the urban canyon and the emitted longwave radiation flux is also larger in the urban area than in the rural area due to the higher urban surface temperature. This contributes to the small difference in net radiation between the urban and rural areas in the daytime. In the nighttime, the net radiation in the urban area is less in its magnitude than that in the rural area due to more emitted longwave radiation in the urban area. In the daytime, the sensible heat flux in the urban area is considerably larger and reaches its peak 90 min later compared to that in the rural area (Fig. 2b). In the nighttime, the sensible heat flux in the urban area is small but not negligible, while the sensible heat flux in the rural area is nearly zero. In the daytime, the latent heat flux in the urban area is considerably smaller than that in the rural area (Fig. 2c) due to the lack of vegetation in the urban area (Taha 1997; Memon et al. 2008). These contrasting daytime sensible and latent heat fluxes between the urban and rural areas are typically observed in cities and their surrounding rural areas (Ramamurthy et al. 2014;

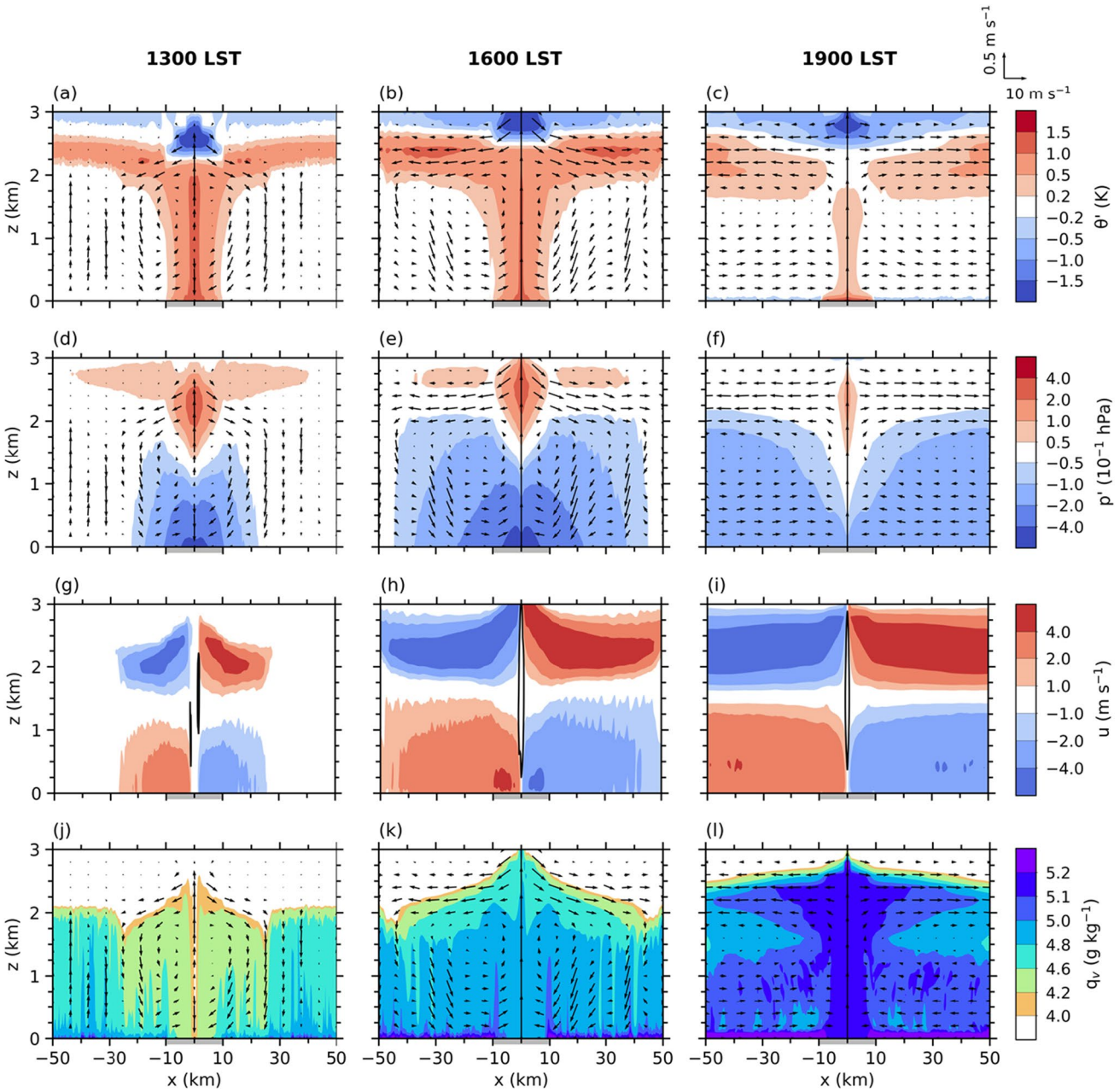


**Fig. 1** Ensemble-mean fields of (**a**, **b**, **c**) potential temperature anomaly, (**d**, **e**, **f**) pressure anomaly, (**g**, **h**, **i**) horizontal velocity, (**j**, **k**, **l**) water vapor mixing ratio, and wind vector (arrow) at 1300 (first column), 1600 (second column), and 1900 LST (third column) for an initial soil moisture content of 0.25 $m^3$ $m^{-3}$. The vertical velocity is shown in (**g**, **h**, **i**) with its contour level of 1.5 m $s^{-1}$. The gray box on the *x* axis represents the urban area

Wang et al. 2015). The urban PBL starts to grow slightly earlier after sunrise and develop deeper than the rural PBL (Fig. 2d). The maximum height of the PBL is 2538 m at 1510 LST in the urban area and 2314 m at 1530 LST in the rural area. The larger sensible heat flux and surface roughness in urban areas are contributing factors for the faster PBL growth and deeper PBL in urban areas than in rural areas (Bowne and Ball 1970; Martilli 2002; Barlow et al. 2015). The PBL height in the rural area decreases very rapidly starting from ~1700 LST and is nearly zero after 1900 LST (Fig. 2d). On the other hand, the PBL height in the urban area decreases gradually after ~1700 LST and remains relatively high in the nighttime. This is due to the small but non-negligible sensible heat flux in the urban area (Fig. 2b).

The 2-m temperature in the urban area is higher than that in the rural area throughout the day, indicating the UHI

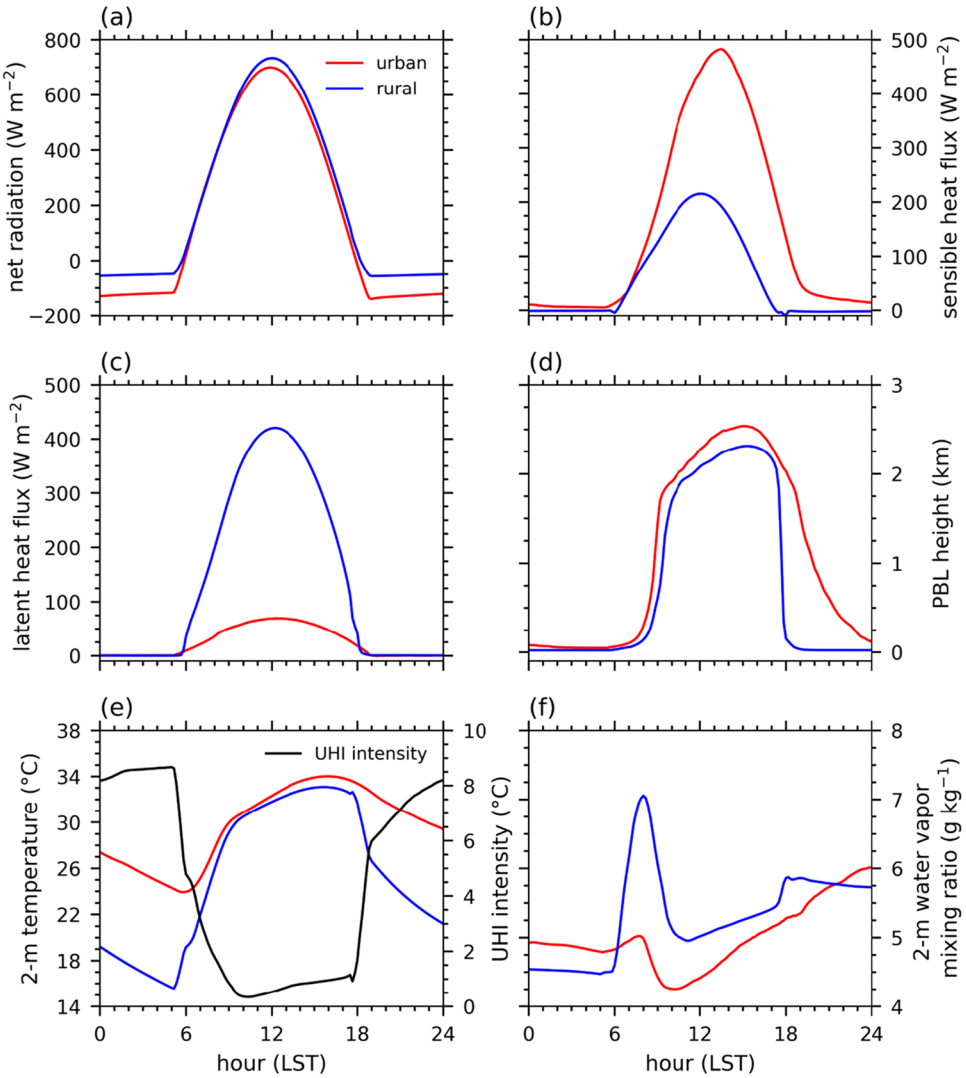


**Fig. 2** Ensemble-mean diurnal variations of (**a**) net radiation, (**b**) sensible heat flux, (**c**) latent heat flux, (**d**) planetary boundary layer height, (**e**) 2-m temperature, and (**f**) 2-m water vapor mixing ratio averaged over the urban (red) and rural (blue) areas for an initial soil moisture content of 0.25 $m^3\ m^{-3}$. The ensemble-mean diurnal variation of urban heat island intensity is also shown in (**e**)

(Fig. 2e). In the morning, the 2-m temperature in the rural area exhibits an earlier and larger increase than that in the urban area. During 0550–1020 LST, the increase in 2-m temperature is 7.17 °C in the urban area and 12.12 °C in the rural area, which decreases the UHI intensity by 4.96 °C. This is likely associated with the shade within the urban area and relatively large thermal admittance of the urban surface (Oke et al. 2017). In the evening, the 2-m temperature exhibits a larger decrease in the rural area than in the urban area. During 1800–1910 LST, the decrease in 2-m temperature is 0.94 °C in the urban area and 5.35 °C in the rural area, which increases the UHI intensity by 4.41 °C. This is to some extent due to the sensible heat flux in the urban area which persists after 1800 LST (Fig. 2c). As a result, the UHI intensity is weak in the daytime and strong in the nighttime, which is consistent with observations (Chow and Roth 2006; Basara et al. 2008; Lee and Baik 2010; Yang et al. 2013). The maximum UHI intensity is 8.67 °C at 0500 LST. The 2-m water vapor mixing ratio in the urban area is smaller than that in the rural area during 0610–2130 LST (Fig. 2f). The 2-m water vapor mixing ratio in the rural area increases rapidly starting from 0550 LST, about one hour after sunrise. This rapid increase is associated with the steep increase in latent heat flux in the rural area (Fig. 2c). Furthermore, the PBL height in the rural area is very low during 0550–0840 LST, inhibiting the vertical mixing of water vapor. This also contributes to the rapid increase in water vapor mixing ratio in the rural area in the morning. During 0800–1020 LST, both 2-m water vapor mixing ratios in the urban and rural areas decrease as the PBL height increases very rapidly (Fig. 2d). Since the evapotranspiration in the rural area continues to occur in the daytime, the 2-m water vapor mixing ratio in the rural area increases gradually during 1110–1720 LST. During this period, the 2-m water vapor mixing ratio in the urban area increases more rapidly than that in the rural area mainly due to the horizontal transport of water vapor from the rural area by the low-level convergent flow of the UBC (Fig. 1). During 1710–1810 LST,

the 2-m water vapor mixing ratio in the rural area rapidly increases by 0.44 g kg$^{-1}$ as the PBL height in the rural area rapidly decreases. After 1810 LST, the 2-m water vapor mixing ratio in the rural area exhibits a slight variation, while that in the urban area gradually increases.

### 3.2 Soil Moisture Impacts on the UHI and UBC

In this subsection, the impacts of changes in soil moisture on the UHI and UBC are examined in detail. The period of 1200–1700 LST, during which the UBC is well developed, is focused. Figure 3 shows the ensemble-mean daytime-averaged UHI and UBC intensities as a function of SM. As SM increases from 0.15 to 0.40 m$^3$ m$^{-3}$, the daytime UHI intensity increases monotonically from 0.3 to 1.1 °C (Fig. 3a). The increase in daytime UHI intensity with increasing soil moisture content agrees with the results of previous studies (Husain et al. 2014; Schlünzen et al. 2023). In the nighttime, the opposite trend, that is, the nighttime UHI intensity decreases with increasing SM, is found (not shown). This also agrees with the results of previous studies (Runnalls and Oke 2000; Schatz and Kucharik 2014; Richard et al. 2021). The rate of increase in daytime UHI intensity decreases with increasing SM, indicating that the impact of increase in soil moisture on the UHI is more pronounced under relatively drier soil conditions.

As SM increases from 0.15 to 0.40 m$^3$ m$^{-3}$, the daytime UBC intensity increases monotonically from 3.1 to 4.5 m s$^{-1}$ (Fig. 3b). The rate of increase in the UBC intensity decreases with increasing SM, consistent with the rate of increase in the UHI intensity (Fig. 3a). The daytime 10-m wind speed in the urban area increases from 1.9 to 3.0 m s$^{-1}$ as SM increases from 0.15 to 0.40 m$^3$ m$^{-3}$. Husain et al. (2014) showed that the daytime near-surface wind speed in an urban area increases when soil moisture increases and that this increase is associated with the change in UBC intensity which results from the increase in UHI intensity. In the last part of this subsection, it will be shown that the increase in daytime UBC intensity increases the daytime UHI intensity by increasing the sensible heat flux in the urban area.

The robustness of the changes in the daytime UHI and UBC intensities with SM is examined. For this, the standard deviations of the daytime UHI and UBC intensities in ensemble members are calculated for each of the experiments with different SM. For all SM, the standard deviations of the daytime UHI intensities are very small (< 0.01 °C). The standard deviations of the daytime UBC intensities are also small (< 0.07 m s$^{-1}$). These results indicate that the overall changes in the daytime UHI and UBC intensities with SM shown in Fig. 3 are not affected by the ensemble spread appearing in each experiment.

Figure 4 shows the ensemble-mean fields of potential temperature anomaly, pressure anomaly, horizontal velocity,

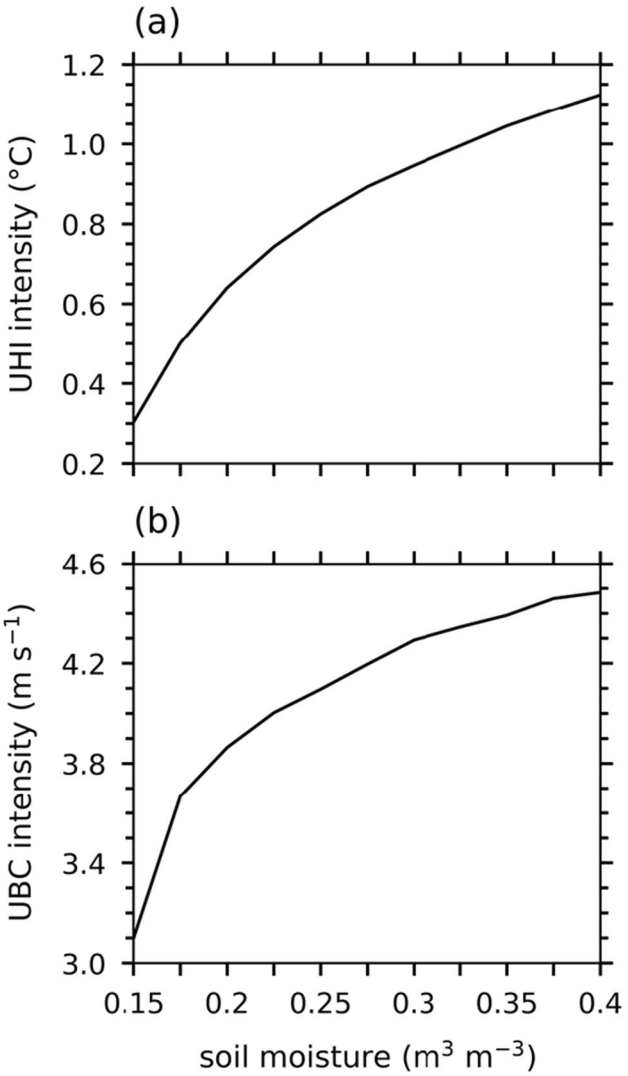


**Fig. 3** Ensemble-mean (**a**) urban heat island intensity and (**b**) urban breeze circulation intensity averaged over 1200–1700 LST as a function of initial soil moisture content

and water vapor mixing ratio averaged over 1200–1700 LST for SM = 0.15, 0.25, and 0.40 m$^3$ m$^{-3}$. As SM increases, the warm anomaly in the urban area and the warm anomaly in the divergent flow region are enhanced (Fig. 4a–c), consistent with the increase in UHI intensity with increasing SM (Fig. 3a). The magnitudes of warm anomaly averaged over $z$ = 0–1 km in the urban area for SM = 0.15, 0.25, and 0.40 m$^3$ m$^{-3}$ are 0.35, 0.66, and 0.79 °C, respectively. Due to the enhanced warm anomaly in the urban area, the negative pressure anomaly there is enhanced with increasing SM (Fig. 4d–f). This leads to stronger low-level convergent flow and accordingly stronger upper-level divergent flow with increasing SM (Fig. 4g–i), consistent with the increase in UBC intensity with increasing SM (Fig. 3b). It is noticeable that the enhanced upper-level divergent flow is more

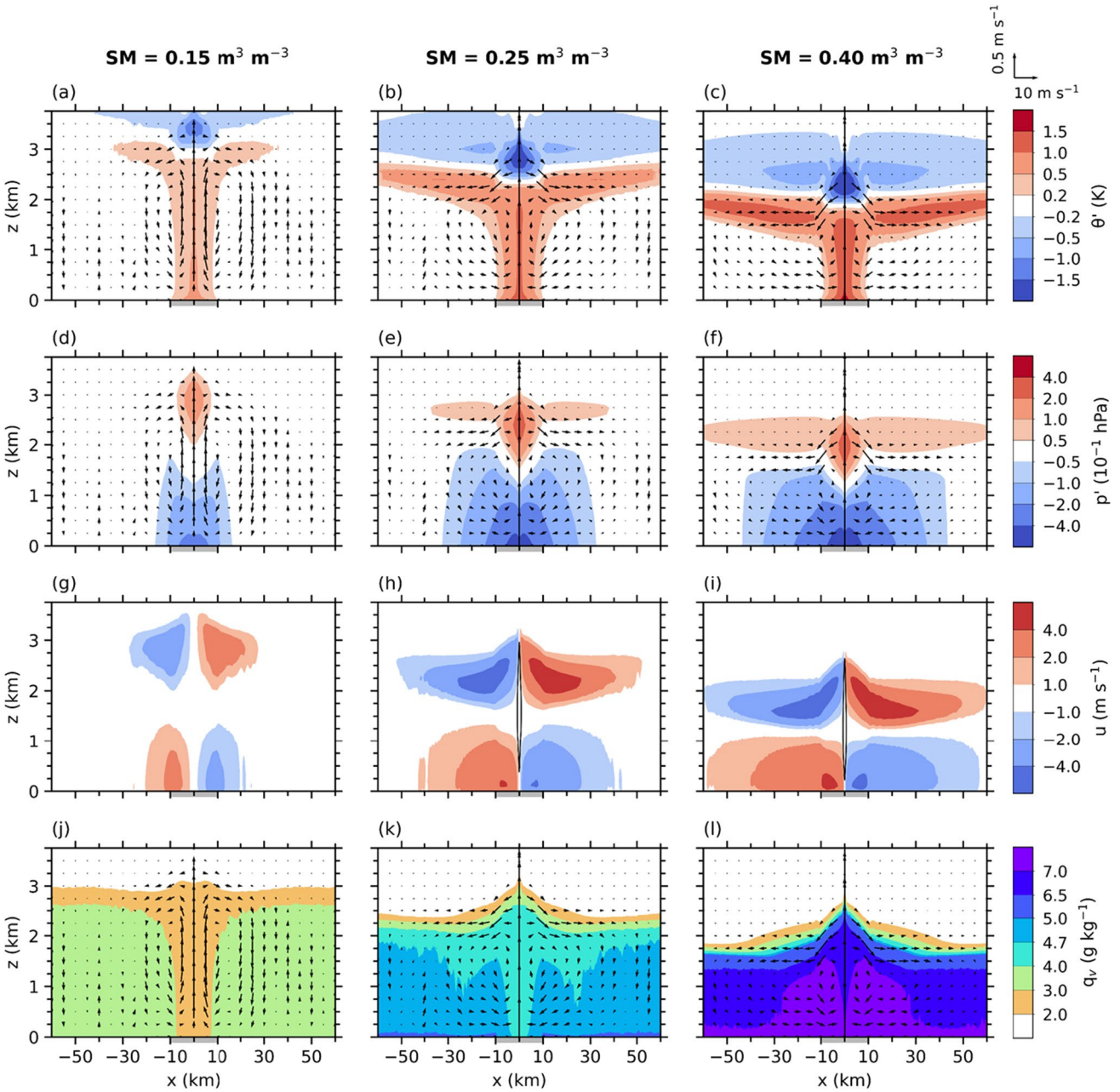


**Fig. 4** Ensemble-mean fields of (**a**, **b**, **c**) potential temperature anomaly, (**d**, **e**, **f**) pressure anomaly, (**g**, **h**, **i**) horizontal velocity, (**j**, **k**, **l**) water vapor mixing ratio, and wind vector (arrow) averaged over 1200–1700 LST for initial soil moisture contents of 0.15 (first column), 0.25 (second column), and 0.40 $m^3\ m^{-3}$ (third column). The vertical velocity contour of 1.5 m $s^{-1}$ is drawn in (**h**, **i**). The gray box on the *x* axis represents the urban area

prominent in its intensity than the enhanced low-level convergent flow. For SM = 0.15 $m^3\ m^{-3}$, two urban breeze fronts are merged at 1630 LST. The horizontal size of the UBC is 40 km (Fig. 4g), and the maximum updraft intensity at the urban center is 0.7 m $s^{-1}$. For SM = 0.25 $m^3\ m^{-3}$, two urban breeze fronts are merged earlier (1350 LST) than those for SM = 0.15 $m^3\ m^{-3}$. The horizontal size of the UBC increases to 75 km (Fig. 4h), and the maximum updraft intensity at the urban center is 3.5 m $s^{-1}$. For SM = 0.40 $m^3\ m^{-3}$, the horizontal size of the UBC further increases to 111 km (Fig. 4i) and the maximum updraft intensity at the urban center is 5.0 m $s^{-1}$. While the horizontal size of the UBC increases with increasing SM, the vertical size of the UBC decreases with increasing SM (Fig. 4g–i). The vertical sizes of the UBC at the urban center for SM = 0.15, 0.25, and 0.40 $m^3\ m^{-3}$ are 3.4, 3.2, and 2.8 km, respectively.

Due to the stronger convergent/divergent flow of the UBC with increasing SM, the water vapor mixing ratio becomes higher in the urban PBL (Fig. 4j–l). For SM = 0.15 $m^3$ $m^{-3}$, below $z \sim 2$ km, the water vapor mixing ratio tends to be smaller in the urban area than in the rural area (Fig. 4j). For SM = 0.25 $m^3$ $m^{-3}$, the transport of relatively moist rural air to the urban area at low levels is enhanced, acting to decrease the difference in water vapor mixing ratio between the urban and rural areas (Fig. 4k). For SM = 0.40 $m^3$ $m^{-3}$, the transport is further enhanced (Fig. 4l). The water vapor mixing ratio is higher in the urban area than in the rural area. As SM increases from 0.15 to 0.40 $m^3$ $m^{-3}$, the water vapor mixing ratio averaged over $z = 0$–1 km in the urban area almost linearly increases from 2.9 to 7.2 g $kg^{-1}$ (figure not shown). These results indicate that the enhanced transport of water vapor from the rural area to the urban area with increasing SM reduces the water vapor deficit or even leads to the water vapor excess in the urban area depending on SM.

Figure 5 shows the ensemble-mean daytime-averaged horizontal advection of potential temperature and water vapor mixing ratio averaged over $z = 0$–1 km in the urban area as a function of SM. The UBC contributes to the decrease in urban air temperature by advecting the relatively cool rural air to the urban area. As SM increases from 0.15 to 0.40 $m^3$ $m^{-3}$, the magnitude of the advective cooling in the urban area increases monotonically from 0.65 to 1.39 K $hr^{-1}$ (Fig. 5a) This is because as SM increases, the difference in potential temperature between the warm urban air and cool rural air increases and the UBC strengthens (Fig. 3). The horizontal advection of water vapor mixing ratio to the urban area also increases from 0.12 to 0.38 g $kg^{-1}$ $hr^{-1}$ as SM increases from 0.15 to 0.40 $m^3$ $m^{-3}$ (Fig. 5b).

The ensemble-mean daytime-averaged vertical profiles of potential temperature and water vapor mixing ratio in the urban and rural areas for SM = 0.15, 0.25, and 0.40 $m^3$ $m^{-3}$ are presented in Fig. 6. The potential temperatures in both the urban and rural areas decrease with increasing SM (Fig. 6a). It is noted that the potential temperature difference between the urban and rural areas increases with increasing SM. The PBL heights in both the urban and rural areas decrease with increasing SM. The PBL height in the urban (rural) area is 2995 (2827), 2449 (2238), and 1880 (1699) m for SM = 0.15, 0.25, and 0.40 $m^3$ $m^{-3}$, respectively. This agrees with the result of Yue et al. (2021) that the increase in soil moisture decreases the PBL height. The decrease in the PBL height is responsible for the decrease in the vertical size of the UBC (Fig. 4g–i). In contrast with the nearly neutral rural PBL, except for the region close to the surface where the atmosphere is unstable, the urban PBL is more stabilized with increasing SM. This is attributed to the enhancement of the low-level advective cooling by the UBC with increasing SM (Fig. 5a). The water vapor mixing ratios

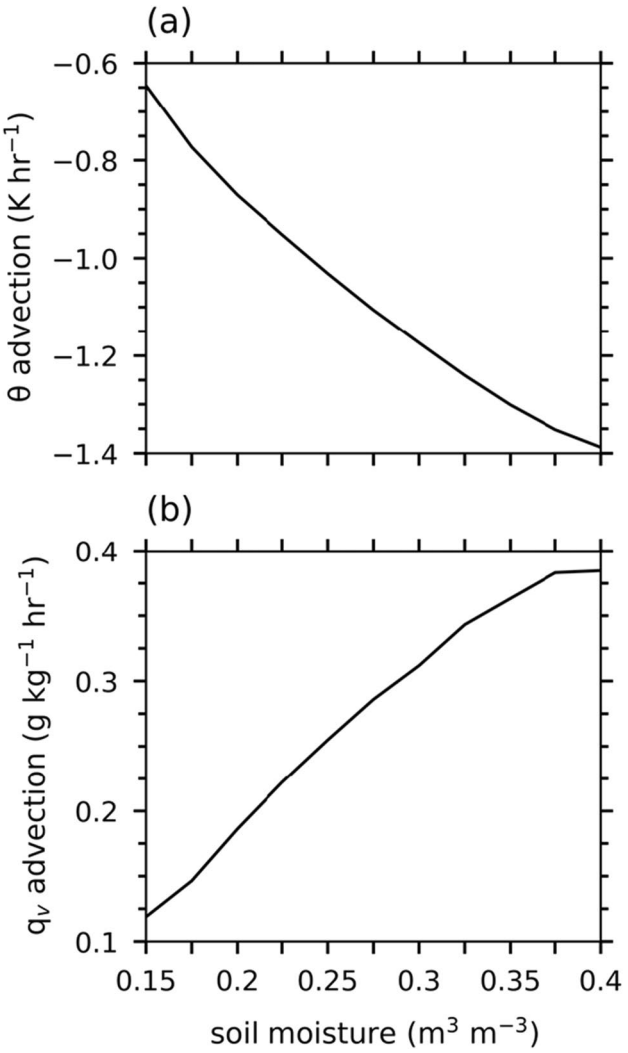


**Fig. 5** Ensemble-mean horizontal advection of (**a**) potential temperature and (**b**) water vapor mixing ratio averaged over $z = 0$–1 km in the urban area as a function of initial soil moisture content. All data are averaged over 1200–1700 LST

in both the urban and rural areas increase with increasing SM (Fig. 6b). For SM = 0.15 $m^3$ $m^{-3}$, the water vapor mixing ratio averaged over $z = 0$–1 km in the urban area is lower by 0.27 g $kg^{-1}$ than that in the rural area. On the other hand, for SM = 0.40 $m^3$ $m^{-3}$, the water vapor mixing ratio averaged over $z = 0$–1 km in the urban area is higher by 0.53 g $kg^{-1}$ than that in the rural area. This is attributed to the increase in the horizontal advection of water vapor (Fig. 5b) and the decrease in PBL height with increasing SM. These results suggest that SM determines whether the urban area is dry or humid compared to the rural area in the daytime.

It has been suggested that the UHI and/or UBC can induce or increase precipitation (Han et al. 2014; Qian et al. 2022), which is another important aspect of urban impacts on local weather and climate. In this study, the UBC and its

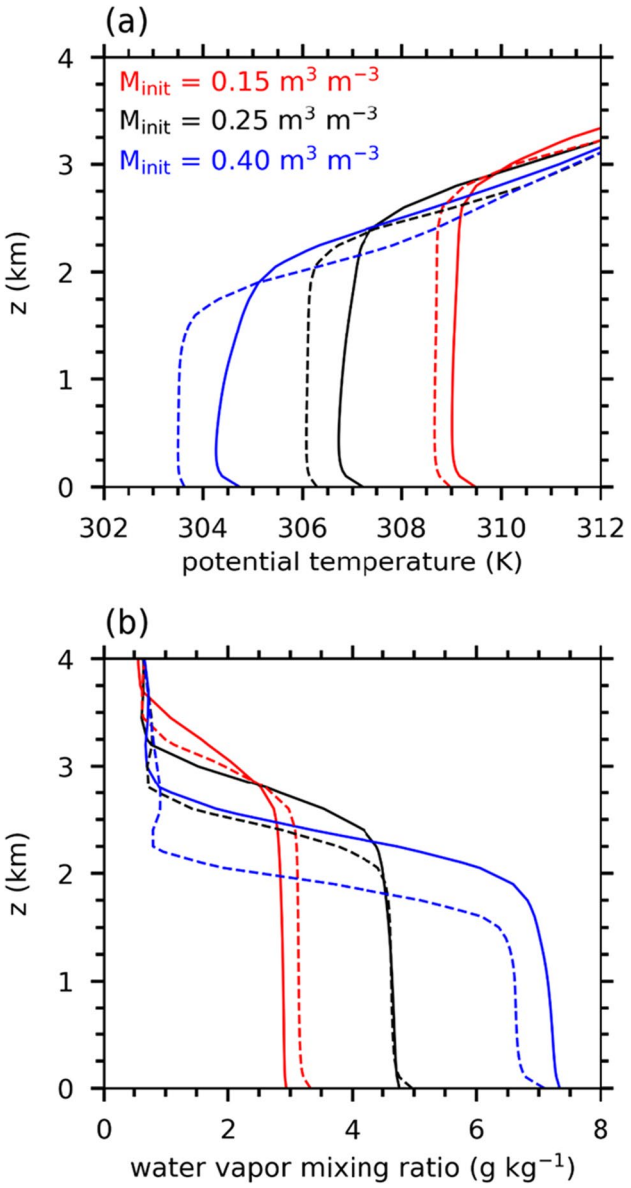


**Fig. 6** Ensemble-mean vertical profiles of (**a**) potential temperature and (**b**) water vapor mixing ratio averaged over the urban (solid) and rural (dashed) areas for initial soil moisture contents of 0.15 (red), 0.25 (black), and 0.40 m$^3$ m$^{-3}$ (blue). All data are averaged over 1200–1700 LST

updraft at the urban center strengthen with increasing SM (Fig. 4g–i). Moreover, as SM increases, the amount of water vapor in the urban area becomes similar to or even larger than that in the rural area (Figs. 4j–l and 6b). These suggest that the urban area could become even more favorable for moist convection initiation than the surrounding rural area under relatively wet soil conditions. This encourages future investigation.

The variations of ensemble-mean daytime-averaged 2-m temperature in the urban and rural areas with SM are shown in Fig. 7a. As SM increases from 0.15 to 0.40 m$^3$ m$^{-3}$, the 2-m temperature in the rural area decreases from 35.4 to 30.0 °C. The 2-m temperature in the urban area also decreases from 35.7 to 31.1 °C mainly due to the enhancement of the advective cooling by the UBC with increasing SM (Fig. 5a). Note that the increase in UHI intensity with increasing SM (Fig. 3a) results from the smaller decrease in 2-m temperature with increasing SM in the urban area than in the rural area (Fig. 7a).

To examine how the increase in soil moisture increases both the daytime UHI intensity and daytime UBC intensity, the variations of ensemble-mean daytime-averaged surface heat fluxes and surface temperature with SM (Fig. 7b–d) are analyzed. As SM increases from 0.15 to 0.40 m$^3$ m$^{-3}$, the latent heat flux in the rural area considerably increases from 218 to 430 W m$^{-2}$ (Fig. 7b). In the urban area, the latent heat flux slightly increases with increasing SM, its difference between SM = 0.15 and 0.40 m$^3$ m$^{-3}$ being 26 W m$^{-2}$. The increase in latent heat flux with the increase in soil moisture is well documented (Schwingshackl et al. 2017). The latent heat flux is caused by transpiration from vegetation and evaporation from soil. An analysis is made on the variations of the transpiration and evaporation with SM (figure not shown). For SM between 0.15 and 0.35 m$^3$ m$^{-3}$, both transpiration from vegetation and evaporation from soil increase with increasing SM in both the urban and rural areas. However, the rate of increase in transpiration from vegetation decreases with increasing SM, while the rate of increase in evaporation from soil slightly increases with increasing SM. For SM between 0.35 (0.375) and 0.40 m$^3$ m$^{-3}$, the transpiration from vegetation very slightly decreases with increasing SM in the rural (urban) area. The little change in transpiration from vegetation under high soil moisture was reported by Verhoef and Egea (2014). Since the decrease in the rate of increase in transpiration from vegetation is more pronounced than the increase in the rate of increase in evaporation from soil, the rate of increase in latent heat flux decreases with increasing SM in both the urban and rural areas for SM between 0.15 and 0.40 m$^3$ m$^{-3}$.

As the latent heat flux in the rural area increases with increasing SM, the sensible heat flux and surface temperature in the rural area considerably decrease with increasing SM (Fig. 7c and d). The decrease in sensible heat flux from the surface with increasing SM in the rural area leads to the decrease in the convergence of sensible heat flux in the near-surface air volume (Oke et al. 2017). Furthermore, the decrease in surface temperature with increasing SM in the rural area leads to the decrease in the convergence of longwave radiative flux in the near-surface air volume due to the reduced emitted longwave radiation from the surface. These result in the considerable decrease in 2-m temperature in the rural area, thereby increasing the UHI intensity (Figs. 3a and 7a). In the urban area, the surface temperature decreases

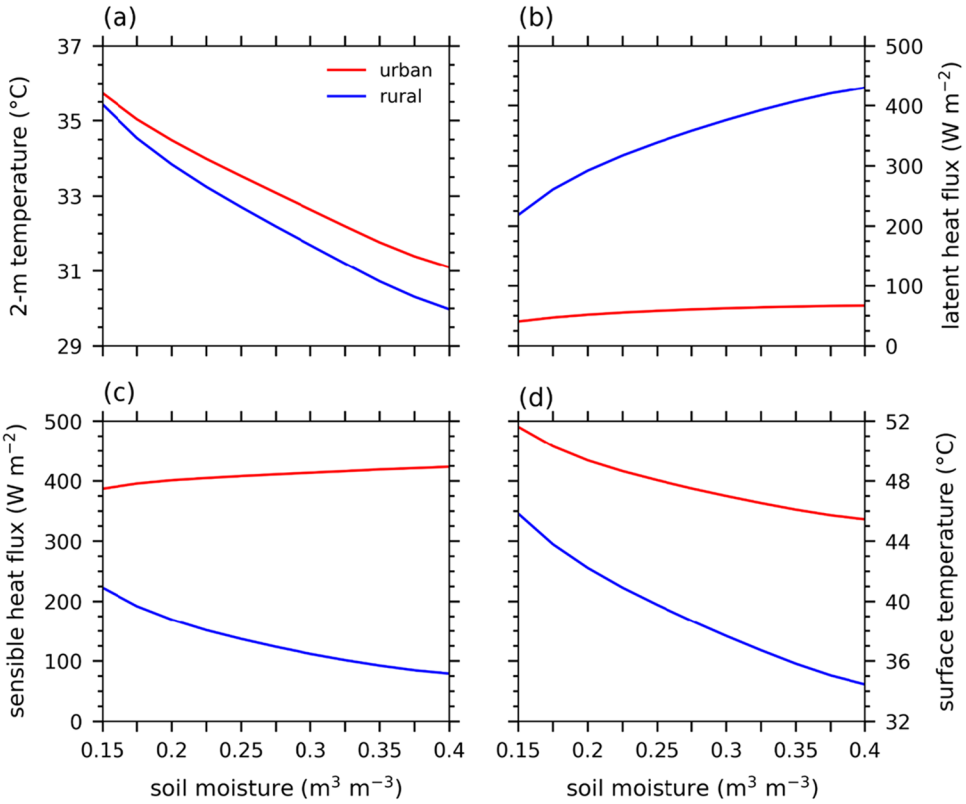


**Fig. 7** Ensemble-mean (**a**) 2-m temperature, (**b**) latent heat flux, (**c**) sensible heat flux, and (**d**) surface temperature averaged over the urban (red) and rural (blue) areas as a function of initial soil moisture content. All data are averaged over 1200–1700 LST

with increasing SM, while interestingly the sensible heat flux slightly increases with increasing SM (Fig. 7c and d). The increases in both sensible and latent heat fluxes with increasing SM in the urban area are responsible for the decrease in surface temperature in the urban area. As SM increases from 0.15 to 0.40 m$^3$ m$^{-3}$, the sensible heat flux in the urban area increases from 387 to 423 W m$^{-2}$. This increase in sensible heat flux further increases the UHI intensity. The increase in near-surface wind speed associated with the increase in UBC intensity with increasing SM (Fig. 3b) is a contributing factor for the increase in sensible heat flux with increasing SM in the urban area. Li et al. (2016) showed that the increase in wind speed increases the urban sensible heat flux and therefore increases the UHI intensity in the daytime. In conclusion, the increase in daytime UHI intensity with increasing SM leads to the increase in daytime UBC intensity which leads to the increase in urban sensible heat flux which in turn leads to the increase in daytime UHI intensity. The positive feedback between the UHI intensity and the UBC intensity is found when soil moisture increases.

It is shown that the increase in the daytime UHI intensity with increasing SM is less pronounced when SM is relatively high (Fig. 3a). This can be associated with the decrease in the rate of increase in rural latent heat flux with increasing SM (Fig. 7b). As discussed above, the increase in latent heat flux in the rural area with increasing SM is the primary factor leading to the increase in the daytime UHI intensity. The less increase in latent heat flux in the rural area when SM is relatively high results in less decreases in sensible heat flux and surface temperature in the rural area (Fig. 7c and d). Hence, the increase in the daytime UHI intensity becomes less when SM increases. The less increase in the daytime UHI intensity leads to the less increase in the daytime UBC intensity. The positive feedback between the UHI intensity and UBC intensity could eventually weaken as well. Finally, it is stated that latitude and season can affect the UHI and UBC intensities. As further study, it would be interesting to investigate to what extent our main results on soil moisture impacts on the UHI and UBC are sensitive to latitude and season.

## 4 Summary and Conclusions

This study examines how changes in soil moisture impact the UHI and UBC. For this, two-dimensional idealized ensemble simulations are performed with different initial soil moisture contents. Main findings are schematically presented in Fig. 8. As soil moisture increases, the latent heat flux increases considerably in the rural area and slightly in the urban area. This results in decreases in sensible heat flux and surface temperature, thus the decrease in rural air temperature. Hence, the UHI intensity and thus UBC intensity increase with increasing soil moisture. Due to the cool

air advection from the rural area to the urban area by the low-level convergent flow of the UBC, the air temperature in the urban area also decreases with increasing soil moisture. Thus, the decrease in air temperature in the urban area with increasing soil moisture results from the decrease in air temperature in the rural area, possibly with a time lag between them. The rate of decrease in air temperature in the urban area is lower than that in the rural area. As the UBC intensity increases, the sensible heat flux in the urban area increases, further increasing the UHI intensity. The positive feedback exists between the increase in UHI intensity and the increase in UBC intensity when soil moisture increases. The decreases in air temperature in both the urban and rural areas cause the PBL height to decrease, hence resulting in the decrease in the vertical size of the UBC with the increase in soil moisture. Due to the increasing UBC intensity with increasing soil moisture, the advection of water vapor from the rural area to the urban area is enhanced. Combined with the decrease in PBL height, this reduces the water vapor deficit or even leads to the water vapor excess in the urban area depending on soil moisture content.

The simulations in this study are conducted in simple settings where an urban area is located on plains and a calm and clear condition is considered. However, various geographical features in and around cities induce local circulations such as sea/land breezes, mountain/valley winds, and river breezes which can influence the UHI and/or UBC (Yoshikado 1992; Ryu and Baik 2013; Yu et al. 2021). In addition, synoptic winds and clouds also affect the developments of UHI, PBL, and local circulations. These influences, which are not considered in this study, can complicate the impacts of changes in soil moisture occurring in cities and therefore deserve investigation. The horizontal grid spacing used in this study belongs to the gray zone resolutions of PBL parameterization (Wyngaard 2004; Shin and Hong 2013). Further study using large-eddy simulations with higher resolutions will be valuable for confirming the soil moisture impacts and also for revealing in detail the turbulent transport processes of momentum, heat, and water vapor.

The PBL height and UBC affect urban air quality by modulating the dispersion and transport of air pollutants and their precursors (Ryu et al. 2013b; Yassin et al. 2018). This study reveals changes in UBC intensity and PBL height with soil moisture. The changes in UBC intensity and PBL height can, to some or a large extent, influence near-surface air pollutant concentrations in the urban area. The enhanced UBC with increasing soil moisture acts to decrease urban near-surface air pollutant concentrations by increasing the transport of relatively clean rural air to the urban area, while the decrease in PBL height with increasing soil moisture acts to increase urban near-surface air pollutant concentrations. These could make the impacts of changes in soil moisture on urban air quality, which encourages investigation. This study reveals significant changes in near-surface temperature and water vapor mixing ratio in the urban area with soil moisture which give implications for urban thermal discomfort, in other words, urban heat stress. The relationship between soil moisture and urban heat stress is complex depending on many factors such as local background climate. This deserves investigation.

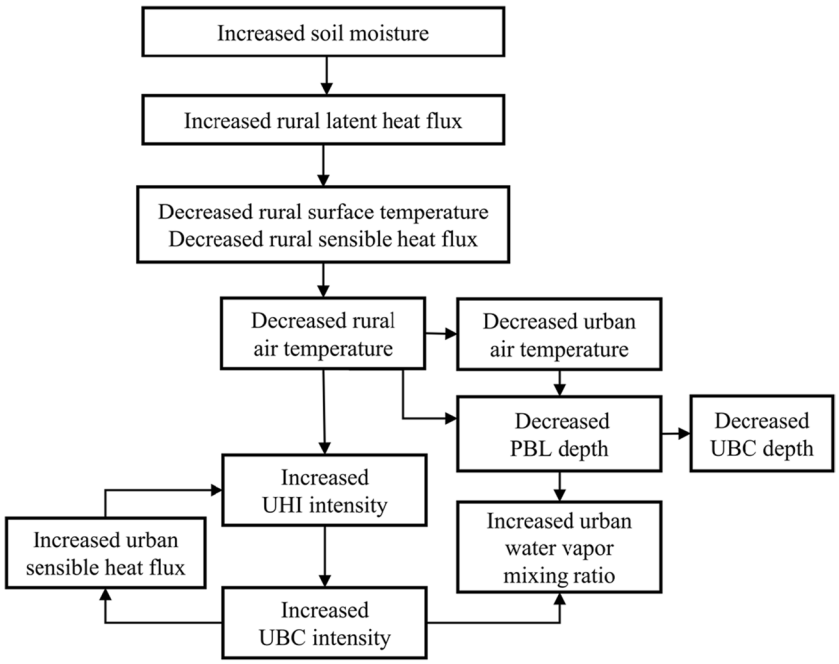


**Fig. 8** Schematic diagram of the impacts of increase in soil moisture on the urban heat island and urban breeze circulation

**Acknowledgements** The authors are sincerely grateful to two anonymous reviewers for providing constructive comments on this work. This work was supported by the National Research Foundation of Korea under grant 2021R1A2C1007044.

**Data Availability** The data that support the findings of this study will be made available upon request.

## Declarations

**Conflict of Interest** The authors declare that they have no conflict of interest.



## References

Arnfield, A.J.: Two decades of urban climate research: a review of turbulence, exchanges of energy and water, and the urban heat island. Int. J. Climatol. **23**, 1–26 (2003)

Barlow, J.F., Halios, C.H., Lane, S.E., Wood, C.R.: Observations of urban boundary layer structure during a strong urban heat island event. Environ. Fluid Mech. **15**, 373–398 (2015)

Basara, J.B., Hall Jr, P.K., Schroeder, A.J., Illston, B.G., Nemunaitis, K.L.: Diurnal cycle of the Oklahoma City urban heat island. J. Geophys. Res. Atmos. **113**, D20109 (2008)

Bowne, N.E., Ball, J.T.: Observational comparison of rural and urban boundary layer turbulence. J. Appl. Meteorol. **9**, 862–873 (1970)

Chow, W.T.L., Roth, M.: Temporal dynamics of the urban heat island of Singapore. Int. J. Climatol. **26**, 2243–2260 (2006)

Cook, B.I., Mankin, J.S., Anchukaitis, K.J.: Climate change and drought: from past to future. Curr. Clim. Chang. Rep. **4**, 164–179 (2018)

Dudhia, J.: Numerical study of convection observed during the Winter Monsoon Experiment using a mesoscale two-dimensional model. J. Atmos. Sci. **46**, 3077–3107 (1989)

Ek, M.B., Holtslag, A.A.M.: Influence of soil moisture on boundary layer cloud development. J. Hydrometeorol. **5**, 86–99 (2004)

Findell, K.L., Eltahir, E.A.B.: Atmospheric controls on soil moisture–boundary layer interactions. Part I: framework development. J. Hydrometeorol. **4**, 552–569 (2003)

Fischer, E.M., Seneviratne, S.I., Lüthi, D., Schär, C.: Contribution of land-atmosphere coupling to recent European summer heat waves. Geophys. Res. Lett. **34**, L06707 (2007)

Ganbat, G., Baik, J.-J., Ryu, Y.-H.: A numerical study of the interactions of urban breeze circulation with mountain slope winds. Theor. Appl. Climatol. **120**, 123–135 (2015)

Grimmond, C.S.B., Oke, T.R.: Heat storage in urban areas: local-scale observations and evaluation of a simple model. J. Appl. Meteorol. **38**, 922–940 (1999)

Guillod, B.P., Orlowsky, B., Miralles, D.G., Teuling, A.J., Seneviratne, S.I.: Reconciling spatial and temporal soil moisture effects on afternoon rainfall. Nat. Commun. **6**, 6443 (2015)

Han, J.-Y., Baik, J.-J., Lee, H.: Urban impacts on precipitation. Asia-Pac. J. Atmos. Sci. **50**, 17–30 (2014)

Hidalgo, J., Masson, V., Pigeon, G.: Urban-breeze circulation during the CAPITOUL experiment: numerical simulations. Meteorol. Atmos. Phys. **102**, 243–262 (2008a)

Hidalgo, J., Pigeon, G., Masson, V.: Urban-breeze circulation during the CAPITOUL experiment: observational data analysis approach. Meteorol. Atmos. Phys. **102**, 223–241 (2008b)

Hirschi, M., Seneviratne, S.I., Alexandrov, V., Boberg, F., Boroneant, C., Christensen, O.B., Formayer, H., Orlowsky, B., Stepanek, P.: Observational evidence for soil-moisture impact on hot extremes in southeastern Europe. Nat. Geosci. **4**, 17–21 (2011)

Hohenegger, C., Brockhaus, P., Bretherton, C.S., Schär, C.: The soil moisture–precipitation feedback in simulations with explicit and parameterized convection. J. Clim. **22**, 5003–5020 (2009)

Hong, S.-Y., Lim, J.-O.J.: The WRF single-moment 6-class microphysics scheme (WSM6). J. Korean Meteorol. Soc. **42**, 129–151 (2006)

Hong, S.-Y., Noh, Y., Dudhia, J.: A new vertical diffusion package with an explicit treatment of entrainment processes. Mon. Weather Rev. **134**, 2318–2341 (2006)

Hong, S.-H., Jin, H.-G., Baik, J.-J.: Impacts of background wind on the interactions between urban breeze circulation and convective cells: ensemble large-eddy simulations. Q. J. R. Meteorol. Soc. **150,** 1518–1537 (2024)

Husain, S.Z., Bélair, S., Leroyer, S.: Influence of soil moisture on urban microclimate and surface-layer meteorology in Oklahoma City. J. Appl. Meteorol. Climatol. **53**, 83–98 (2014)

Jiménez, P.A., Dudhia, J., González-Rouco, J.F., Navarro, J., Montávez, J.P., García-Bustamante, E.: A revised scheme for the WRF surface layer formulation. Mon. Weather Rev. **140**, 898–918 (2012)

Klemp, J.B., Dudhia, J., Hassiotis, A.D.: An upper gravity-wave absorbing layer for NWP applications. Mon. Weather Rev. **136**, 3987–4004 (2008)

Lee, S.-H., Baik, J.-J.: Statistical and dynamical characteristics of the urban heat island intensity in Seoul. Theor. Appl. Climatol. **100**, 227–237 (2010)

Lemonsu, A., Masson, V.: Simulation of a summer urban breeze over Paris. Bound.-Layer Meteorol. **104**, 463–490 (2002)

Li, D., Sun, T., Liu, M., Wang, L., Gao, Z.: Changes in wind speed under heat waves enhance urban heat islands in the Beijing metropolitan area. J. Appl. Meteorol. Climatol. **55**, 2369–2375 (2016)

Liu, J., Pu, Z.: Does soil moisture have an influence on near-surface temperature? J. Geophys. Res. Atmos. **124**, 6444–6466 (2019)

Martilli, A.: Numerical study of urban impact on boundary layer structure: sensitivity to wind speed, urban morphology, and rural soil moisture. J. Appl. Meteorol. **41**, 1247–1266 (2002)

Memon, R.A., Leung, D.Y.C., Liu, C.: A review on the generation, determination and mitigation of Urban Heat Island. J. Environ. Sci. **20**, 120–128 (2008)

Mlawer, E.J., Taubman, S.J., Brown, P.D., Iacono, M.J., Clough, S.A.: Radiative transfer for inhomogeneous atmospheres: RRTM, a validated correlated-k model for the longwave. J. Geophys. Res. Atmos. **102**, 16663–16682 (1997)

Oke, T.R.: The urban energy balance. Prog. Phys. Geogr. **12**, 471–508 (1988)

Oke, T.R., Mills, G., Christen, A., Voogt, J.A.: Urban Climates. Cambridge University Press, Cambridge (2017)

Pan, H.-L., Mahrt, L.: Interactions between soil hydrology and boundary-layer development. Bound.-Layer Meteorol. **38**, 185–202 (1987)

Piringer, M., Joffre, S., Baklanov, A., Christen, A., Deserti, M., De Ridder, K., Emeis, S., Mestayer, P., Tombrou, M., Middleton, D.,

Baumann-Stanzer, K., Dandou, A., Karppinen, A., Burzynski, J.: The surface energy balance and the mixing height in urban areas—activities and recommendations of COST-Action 715. Bound.-Layer Meteorol. **124**, 3–24 (2007)

Qian, Y., Chakraborty, T.C., Li, J., Li, D., He, C., Sarangi, C., Chen, F., Yang, X., Leung, L.R.: Urbanization impact on regional climate and extreme weather: current understanding, uncertainties, and future research directions. Adv. Atmos. Sci. **39**, 819–860 (2022)

Ramamurthy, P., Bou-Zeid, E.: Heatwaves and urban heat islands: a comparative analysis of multiple cities. J. Geophys. Res. Atmos. **122**, 168–178 (2017)

Ramamurthy, P., Bou-Zeid, E., Smith, J.A., Wang, Z., Baeck, M.L., Saliendra, N.Z., Hom, J.L., Welty, C.: Influence of subfacet heterogeneity and material properties on the urban surface energy budget. J. Appl. Meteorol. Climatol. **53**, 2114–2129 (2014)

Ramamurthy, P., Li, D., Bou-Zeid, E.: High-resolution simulation of heatwave events in New York City. Theor. Appl. Climatol. **128**, 89–102 (2017)

Richard, Y., Pohl, B., Rega, M., Pergaud, J., Thevenin, T., Emery, J., Dudek, J., Vairet, T., Zito, S., Chateau-Smith, C.: Is Urban Heat Island intensity higher during hot spells and heat waves (Dijon, France, 2014–2019)? Urban Clim. **35**, 100747 (2021)

Runnalls, K.E., Oke, T.R.: Dynamics and controls of the near-surface heat island of Vancouver, British Columbia. Phys. Geogr. **21**, 283–304 (2000)

Ryu, Y.-H., Baik, J.-J.: Daytime local circulations and their interactions in the Seoul metropolitan area. J. Appl. Meteorol. Climatol. **52**, 784–801 (2013)

Ryu, Y.-H., Baik, J.-J., Lee, S.-H.: A new single-layer urban canopy model for use in mesoscale atmospheric models. J. Appl. Meteorol. Climatol. **50**, 1773–1794 (2011)

Ryu, Y.-H., Baik, J.-J., Han, J.-Y.: Daytime urban breeze circulation and its interaction with convective cells. Q. J. R. Meteorol. Soc. **139**, 401–413 (2013a)

Ryu, Y.-H., Baik, J.-J., Kwak, K.-H., Kim, S., Moon, N.: Impacts of urban land-surface forcing on ozone air quality in the Seoul metropolitan area. Atmos. Chem. Phys. **13**, 2177–2194 (2013b)

Santamouris, M.: Analyzing the heat island magnitude and characteristics in one hundred Asian and Australian cities and regions. Sci. Total Environ. **512–513**, 582–598 (2015)

Schatz, J., Kucharik, C.J.: Seasonality of the urban heat island effect in Madison, Wisconsin. J. Appl. Meteorol. Climatol. **53**, 2371–2386 (2014)

Schlünzen, K.H., Grimmond, S., Baklanov, A.: Guidance on Measuring, Modelling, and Monitoring the Canopy Layer Urban Heat Island (CL-UHI). World Meteorological Organization, Geneva (2023)

Schwingshackl, C., Hirschi, M., Seneviratne, S.I.: Quantifying spatiotemporal variations of soil moisture control on surface energy balance and near-surface air temperature. J. Clim. **30**, 7105–7124 (2017)

Seneviratne, S.I., Corti, T., Davin, E.L., Hirschi, M., Jaeger, E.B., Lehner, I., Orlowsky, B., Teuling, A.J.: Investigating soil moisture–climate interactions in a changing climate: a review. Earth-Sci. Rev. **99**, 125–161 (2010)

Shin, H.H., Hong, S.-Y.: Analysis of resolved and parameterized vertical transports in convective boundary layers at gray-zone resolutions. J. Atmos. Sci. **70**, 3248–3261 (2013)

Skamarock, W.C., Klemp, J.B., Dudhia, J., Gill, D.O., Liu, Z., Berner, J., Wang, W., Powers, J.G., Duda, M.G., Barker, D.M., Huang, X.-Y.: A description of the advanced research wrf model version 4. NCAR Tech. Note NCAR/TN-556+STR, pp. 145 (2019)

Taha, H.: Urban climates and heat islands: albedo, evapotranspiration, and anthropogenic heat. Energy Build. **25**, 99–103 (1997)

Tewari, M., Chen, F., Wang, W., Dudhia, J., LeMone, M.A., Mitchell, K., Ek, M., Gayno, G., Wegiel, J., Cuenca, R.H.: Implementation and verification of the unified Noah land surface model in the WRF model. 20th Conference on Weather Analysis and Forecasting/16th Conference on Numerical Weather Prediction, Seattle (2004)

Verhoef, A., Egea, G.: Modeling plant transpiration under limited soil water: comparison of different plant and soil hydraulic parameterizations and preliminary implications for their use in land surface models. Agric. For. Meteorol. **191**, 22–32 (2014)

Wang, L., Gao, Z., Miao, S., Guo, X., Sun, T., Liu, M., Li, D.: Contrasting characteristics of the surface energy balance between the urban and rural areas of Beijing. Adv. Atmos. Sci. **32**, 505–514 (2015)

Wyngaard, J.C.: Toward numerical modeling in the "terra incognita." J. Atmos. Sci. **61**, 1816–1826 (2004)

Xu, W., Yuan, W., Dong, W., Xia, J., Liu, D., Chen, Y.: A meta-analysis of the response of soil moisture to experimental warming. Environ. Res. Lett. **8**, 044027 (2013)

Yang, P., Ren, G., Liu, W.: Spatial and temporal characteristics of Beijing urban heat island intensity. J. Appl. Meteorol. Climatol. **52**, 1803–1816 (2013)

Yassin, M.F., Al-Shatti, L.A., Al Rashidi, M.S.: Assessment of the atmospheric mixing layer height and its effects on pollutant dispersion. Environ. Monit. Assess. **190**, 372 (2018)

Yoshikado, H.: Numerical study of the daytime urban effect and its interaction with the sea breeze. J. Appl. Meteorol. **31**, 1146–1164 (1992)

Yu, B., Zhu, B., Miao, S., Kang, H., He, X., Liu, H., Liang, Z., Chen, F.: Observational signal of the interaction between mountain–plain wind and urban breeze under weak synoptic systems. J. Geophys. Res. Atmos. **126**, e2020JD032809 (2021)

Yue, M., Wang, M., Guo, J., Zhang, H., Dong, X., Liu, Y.: Long-term trend comparison of planetary boundary layer height in observations and CMIP6 models over China. J. Clim. **34**, 8237–8256 (2021)